Hindawi Publishing Corporation
International Journal of Distributed Sensor Networks
Volume 2015, Article ID 531516, 7 pages
http://dx.doi.org/10.1155/2015/531516

Research Article

Acquisition and Monitoring System for TEG Characterization

O. H. Ando Jr.,[1] C. L. Izidoro,[1] J. M. Gomes,[2] J. H. Correia,[2] J. P. Carmo,[3] and L. Schaeffer[1]

[1]*Federal University of Rio Grande do Sul (UFRGS), Mechanics Laboratory Transformation-LdTM, Campus do Vale, 91501-970 Porto Alegre, RS, Brazil*
[2]*Department of Industrial Electronics, University of Minho, Campus Azurem, 4800-058 Guimarães, Portugal*
[3]*Department of Electrical Engineering (SEL), University of São Paulo (USP), Avenida Trabalhador São-Carlense 400, Parque Industrial Arnold Schimidt, 13566-590 São Carlos, SP, Brazil*

Correspondence should be addressed to J. P. Carmo; jcarmo@sc.usp.br

Received 25 July 2014; Accepted 20 August 2014

Academic Editor: Luis M. Gonçalves

This paper presents an acquisition system for measuring and characterization of thermoelectric generators (TEGs) for energy harvesting purposes on wireless sensors networks (WSNs). This system can monitor and characterize up to three TEGs simultaneously and is comprised of two main electronic circuits: the first one is composed of 12 input channels being three for reading voltage, three for reading current by making use of instrumentation amplifiers (ACS712), and six thermocouples for signal reading (<400°C). The second electronic circuit consists of a proportional-integral-derivative (PID) controller with two pulse width modulation (PWM) input channels for controlling the heat (thermoresistance) and cooling (controlled cooler) sources, respectively, following a predefined temperature gradient. The TEG measured data for the voltage, current, and temperature can be acquired in real-time with an application written on Delphi language and displayed both through a numeric and graphical display. In order to validate the precision and accuracy two commercial TEG modules (inbC1-127.08HTS) compatible with temperatures up to 200°C without signal degradation were used in series. The functional prototype of the implemented system had a cost under ≈430 USD, making it suitable where a good knowledge of the electrical characteristics of TEGs is of major interest, especially on cogeneration systems.

1. Introduction

In the present days, the search for new energy sources is mandatory in order to respond to continuous demand for electric energy [1, 2]. Among all the energy sources currently available, renewable energy [3, 4] and residual energy scavenging from industrial processes [5, 6] are presented as viable options. This is not strange, when looking at the increasing interest of ubiquitous electronic devices in the everyday life of human-being. Moreover, the complexity and requirements of these devices are not bounded by strict limits, which means that the use of batteries cannot be enough to ensure an uninterruptible working cycle. Therefore, the operational integration of such devices with some kind of energy recovering systems can reveal an interesting approach. This is the main reason behind the growth in the use of external (and renewable) energy sources for powering the devices with a process known as energy harvesting [7–24]. Regarding the latter, the use of materials presenting thermoelectric properties due to the Seebeck effect makes possible the conversion of thermal energy into electric energy [25] with an efficiency of 5–7% [26]. The efficiency follows a close relation to the Figure-of-Merit, ZT (dimensionless), which is conditioned by three factors: Seebeck coefficient, α [VK^{-1}], low electric resistivity, ρ [Ωm], and low thermal conductivity, κ [$Wm^{-1}K^{-1}$] [27, 28]. Another performance factor is more appropriate on TEGs: the power factor (PF [$WK^{-2}m^{-1}$]). The PF is defined as the electric power per unit of area through which the heat flows, per unit of temperature gradient between the hot and the cold sides. These quantities, for example, ZT (dimensionless) and PF, are, respectively, given by the well-known formulas [29, 30]:

$$ZT = \frac{\alpha^2 T}{\rho\kappa}, \qquad \mathrm{PF} = \frac{\alpha^2}{\rho}\left[\mathrm{WK^{-2}\,m^{-1}}\right]. \tag{1}$$

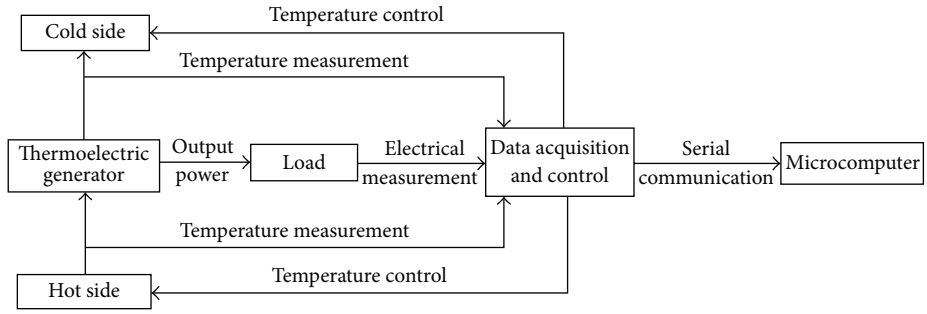

Figure 1: Data acquisition and control system architecture.

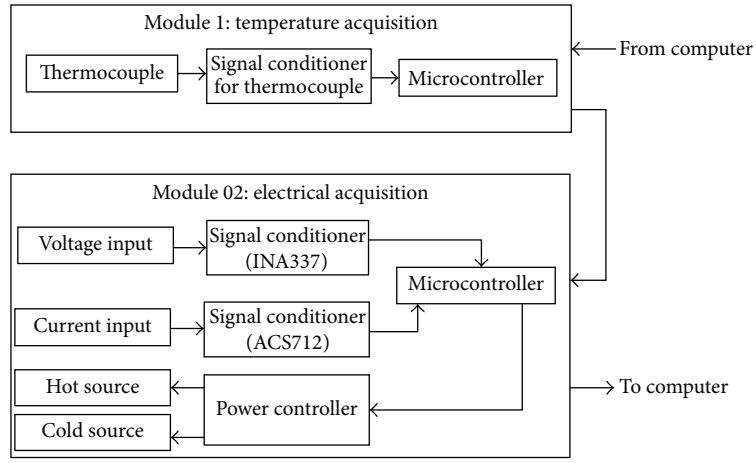

Figure 2: Acquisition hardware.

Recent researches presented efficiencies higher than 20% by using new techniques in the development of thermoelectric materials [31, 32]. In the face of these developments, the use of TEGs as power sources by harvesting thermal energy from the cogeneration losses on fabrication plants, transforming it into electrical energy [33, 34], is expected. In this context, a monitoring and acquisition system for TEG characterization is presented, comprised by thermal system with heating and cooling capabilities and a data acquisition and monitoring system for temperature, voltage, current, and power. The resulting data is then acquired and presented in real time by software developed in Delphi language, making possible the visualization and study of the thermoelectric material properties by plotting its efficiency curves. Finally this system is validated against two inbC1-127.08HTS from Thermoelectric Power Generation connected in series.

2. System Architecture

The acquisition and control system is implemented with a microcontroller capable of acquiring the data signals from the thermoelectric modules: temperature, voltage, current, and power. The following stage offers a PID controller compatible with two PWM control signals for setting the heat and cooling sources, by thermoresistance and controlled cooler, respectively, in order to follow the thermal gradient predefined test parameters. The development of a Delphi running software, capable of data acquisition and monitoring, plots graphics for each of the variables being measured. Figure 1 presents the diagram for the data acquisition system.

The use of this integrated system also offers the advantage of reducing the necessity of using equipment with different task capabilities for reading and presenting the data that is usually involved in these procedures, thus simplifying the process. The acquisition software saves the data onto hard drive disc from where it can be printed or exported to other software for analysis purposes making possible the comparison with previous tests.

The use of a universal serial bus (USB) to serial communication hardware makes possible the use of any personal laptop computer as an acquisition tool, with the previous communication driver install being only necessary.

2.1. Hardware. The acquisition hardware offers six channels for temperature reading (<400°C), three for current (<20 A) and three for voltage (<24 V_{dc}) making a total of twelve input channels. Moreover the voltage channels offer the option for differential readings for each individual thermoelectric module by using separate voltage references.

The acquisition hardware diagram, shown in Figure 2, is divided into two main modules: the first one is responsible for temperature reading while the second for reading the electric signals and controlling the heat and cooling sources. These sources are then controlled by two PWM signals generated by

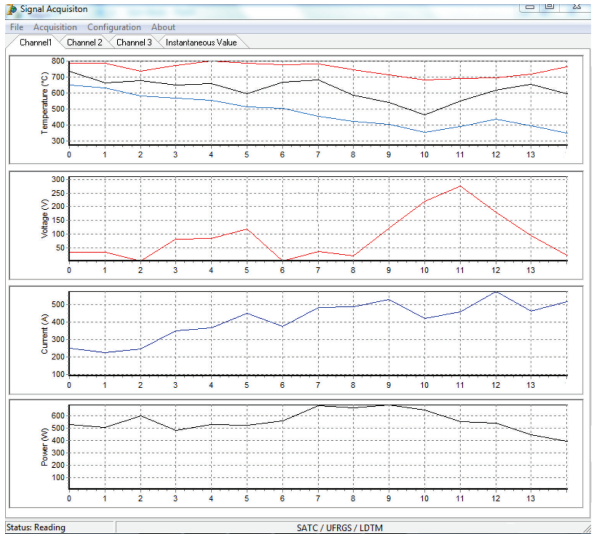

Figure 3: Software main screen showing plotted data.

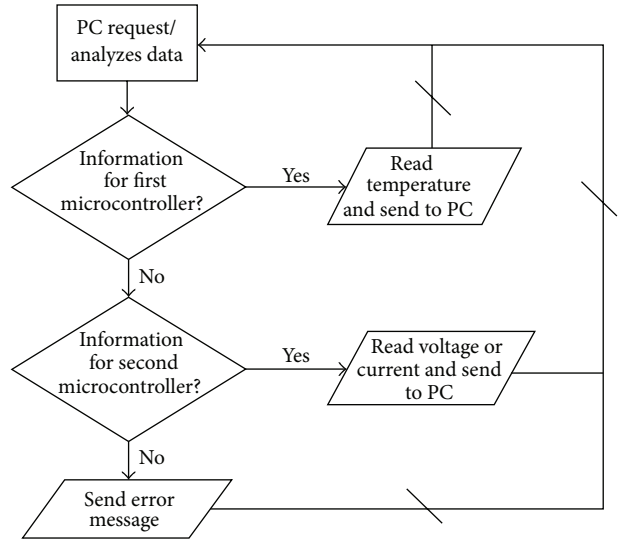

Figure 4: Flowchart for the communication protocol.

a PID controller previously calibrated guaranteeing control precision for the temperature.

The modular acquisition system with noncentralized architecture enables the independent selection of each individual channel. The configuration is done via software by enabling or disabling each channel according to the test parameters.

2.2. Software. Data from the acquisition hardware is handled by a computer running a custom software developed in Borland Delphi 7.0 graphical development environment. In the software menus it is possible to enable or disable each individual channel, select the temperature gradient required for the test, and generate data reports. The dynamic graphical data presentation can also be stored in archives for future analysis.

Figure 3 shows the acquisition data software main screen: from top to bottom in the first graph the temperatures in ˚C for the heat source (red top line), the low temperature source (blue lower line), and the temperature differential (black middle line) are plotted. In the second, third, and fourth graphs the data for voltage, current, and power is plotted.

The communication between the devices is managed by the computer which starts by requesting data from the acquisition hardware. If the computer requests the temperature reading, the first module sends the request. If the request is for the voltage or current, the first module bypasses the request to the second module which returns the information accordingly. At last, the computer sets the temperature by sending the control signals for the thermal (heat and cold) sources. Figure 4 shows the communication flowchart.

3. Experimental

By maintaining a constant temperature differential on opposite sides of a thermoelectric material current flow is generated and a voltage differential builds up. In order to study the characteristics and performance of a thermoelectric device, a device capable of maintaining a controlled and precise temperature differential by actuating a heat and cool sources, resulting in a TEG response curve behavior, is required.

3.1. Measurement Setup. The TEG test setup assembled is shown in Figure 5. The heat resistor is positioned under the TEG for rising the temperature of one side while on the top is placed a heat sink assisted by a cooler for lowering the temperature. This ensures a constant temperature differential on opposite sides of the TEG.

Two sheets of aluminium are used: one placed between the heating resistor and the TEG, while the other between the TEG and the heat sink. This provides an even temperature on both TEG surfaces and an attachment point for thermocouples. The data was acquired by the previously described system aided by a computer running the custom software. Figure 6 shows the schematic for the complete system.

In order to plot the TEG characteristic curves, a temperature gradient (ΔT) sweep from 5˚C to 80˚C with 5˚C increment steps was conducted. From the stipulated temperature gradient was calculated, via software, the control signals for both the heat and cooling sources. A temperature closed loop feedback was implemented providing precision by using one of the three temperature reading channels. This ensures a stable final temperature differential value for each step by actuating both the heat and cool sources with PWM commands. The software displays a visual notification when temperature gradient reaches a constant value ensuring the stability test.

Real-time measurement takes place for the temperature differential, voltage, and current by activating the respective reading channels. This synchronized reading for the variables can be visualized, also in real time, on the computer. By using the extra reading channels it is possible to acquire the temperature, voltage, and current at distinct places among the modules.

This procedure was conducted for all temperature gradients, from 5˚C to 80˚C, for two separate procedures: in

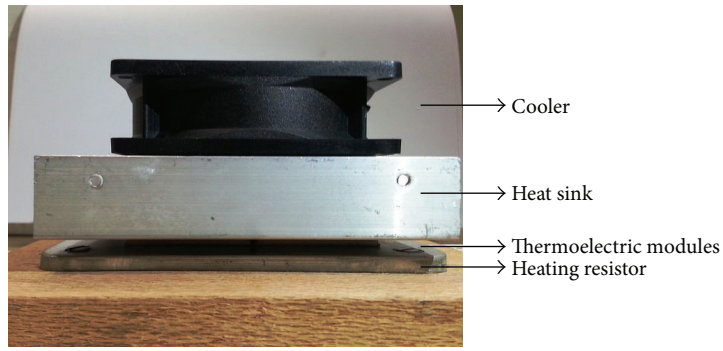

Figure 5: Experimental setup.

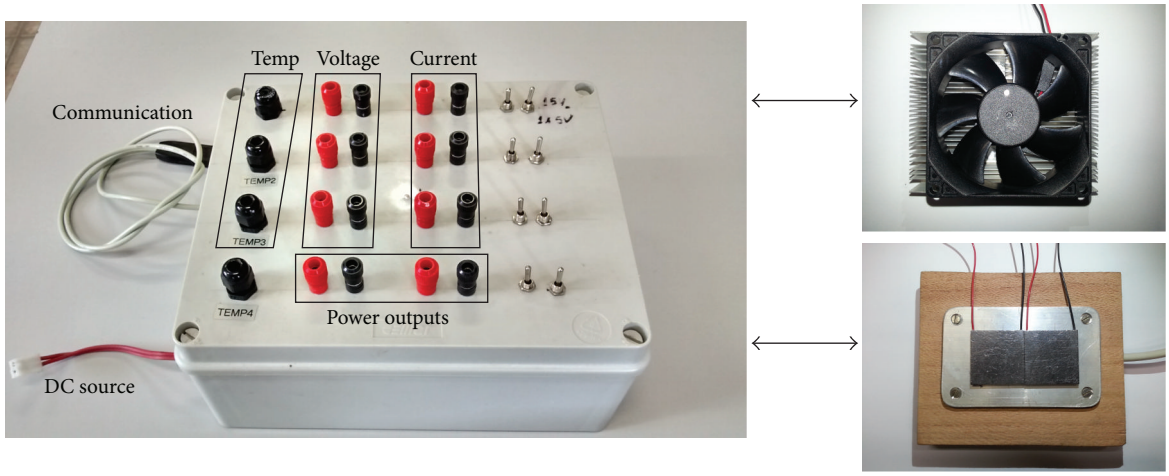

Figure 6: Setup used to connect the acquisition system into the TEGs.

the first sixteen tests, were performed without any load, with the temperature gradient and output voltage only being measured. In the second another sixteen tests, took place but with a resistive load attached to the TEG output. The measured variables were the temperature gradient, voltage, and current.

The performed tests revealed a precision of ±1%, ±1.5%, and ±1.4% for the temperature, voltage, and current, respectively, with a maximum error of 1%. These values were obtained after comparing both the setup performance and a calibrated hardware performance. Adjustments via software were made after using data analysis tools based on ordinary least squares (OLS) and linear equations.

For every test procedure the sampled data generated several different files with temperature values for the heated side, cooled side, temperature gradient, voltage, current, and electric power. These files were exported to a spreadsheet for data treatment in order to obtain a graphical output the current software cannot plot.

3.2. Measurement Results. This chapter validates the use of the two inbC1-127.08HTS connected in series by analysing the test results. The open voltage, V_{out}, procedure determines the output open voltage value for each temperature gradient value, ΔT. Figure 7 shows the graphic obtained data analysis of the open voltage procedure.

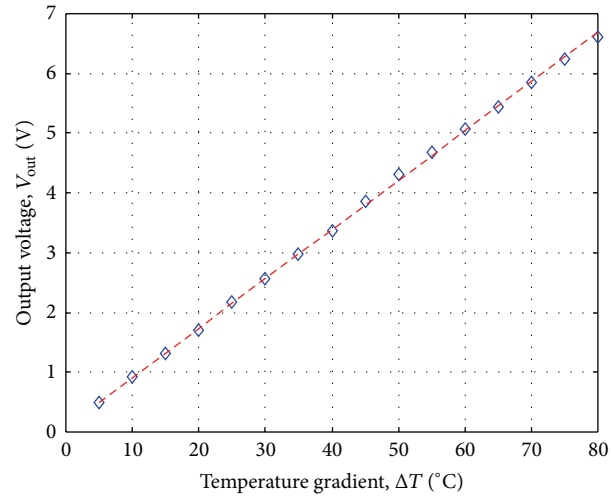

Figure 7: The open circuit voltage, V_{out} [V], as function of the temperature gradient, ΔT [°C].

Based on data presented on Figure 7, the generated voltage constantly varies with the temperature gradient. For temperature gradients ΔT in the range 5 to 80°C, the following equation is obtained after applying the OLS for all the output

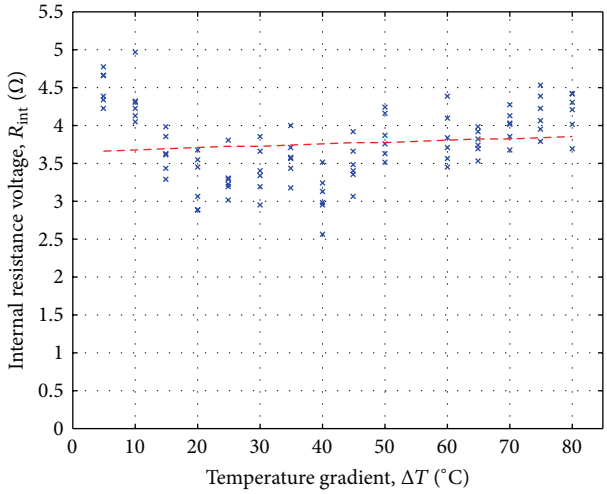

FIGURE 8: The internal resistance of TEG, R_{int} [Ω], as function of the temperature gradient, ΔT [°C].

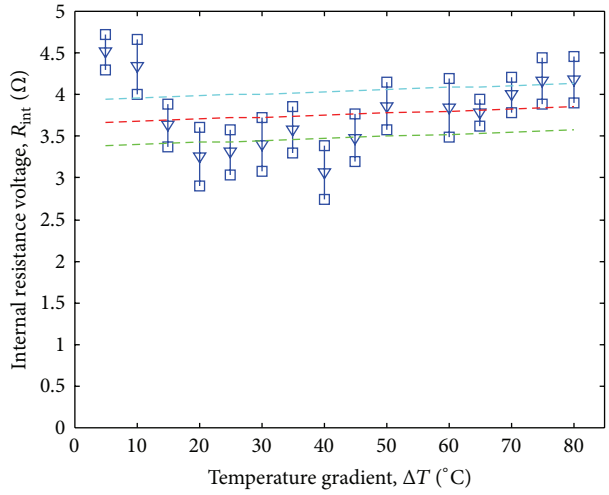

FIGURE 9: The medium and standard deviation values of the internal resistance of TEG, R_{int} [Ω], as function of the temperature gradient, ΔT [°C].

voltage samples: $V_{out} = 78.6 + 82.7 \times \Delta T$ [mV]. The dashed red line with respect to the linear regression adjusts perfectly to the measurements (blue diamonds) with a measured correlation coefficient of 99.97%.

Comparing the data samples with the tendency line it is clear that for every sample the relation V/I follows the same variation rate, which translates into a constant internal thermoelectric module resistance regarding the temperature at which the test took place making possible the determination of the internal resistance (Figure 8) for the group of thermoelectric modules. The dashed red line in Figure 8 was obtained by considering the mean $R_{int}(\Delta T)$ of individual values of $R_{int,k}$, $k = 1, \ldots, 6$, for each temperature gradient ΔT. Then, the latter line was obtained by linear regression of these individual $R_{int}(\Delta T)$'s. The line is defined as $R_{int} = R_{int,0} + R_{int,\Delta} \times \Delta T$, where $R_{int,0} = 3.66\,\Omega$ and $R_{int,\Delta} = 2.5\,\text{m}\Omega/^{\circ}\text{C}$. This gives a mean range of temperature gradients around 40°C of $R_{int,\text{mean-range-}\Delta T} = 3.76\,\Omega$.

In Figure 9, the triangles represent the mean value ($\mu_{\Delta T}$) of R_{int} (the values represented by the blue ×s in Figure 8) for that specific ΔT, while the distances into the squares are the standard deviation $\sigma_{\Delta T}$ for that specific ΔT. Thus, for each ΔT, the central triangle identifies the internal resistance average, $R_{int\_mean,\Delta T}$. Figure 9 also shows the average line (dashed red line in the middle) for the internal resistance average value $R_{int\_mean,\Delta T}$, showing that it varies linearly with the increment of the temperature gradient, ΔT. For the sample universe, the mean value of these 15 different values of $R_{int\_mean,\Delta T}$ is equal to $(\mu_{5^{\circ}} + \mu_{10^{\circ}} + \cdots + \mu_{80^{\circ}})/15 \approx 3.76\,\Omega$, while the mean value of $\sigma_{\Delta T}$ (for each ΔT) is equal to $(\sigma_{5^{\circ}} + \sigma_{10^{\circ}} + \cdots + \sigma_{80^{\circ}})/15 \approx 0.28\,\Omega$. Hereby, it is possible to obtain the internal resistance of $3.76\,\Omega$ with deviation of $0.28\,\Omega$ resulting in $R_{int} = R_0 \pm \Delta R_{int} = 3.76 \pm 0.28\,\Omega$ for the series modules. In Figure 9, the distances between the dashed cyan (top line) and green lines (bottom line) with respect to the dashed red line in the middle are equal to $0.28\,\Omega$.

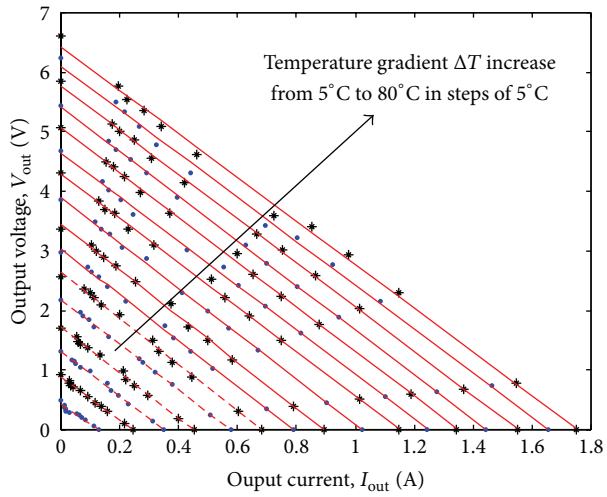

FIGURE 10: The output voltage, V_{out} [V], versus the output current, I_{out} [A], for different temperature gradient, ΔT [°C].

By using a fixed resistive load value (Figure 10) for different temperature gradients ($\Delta T = T_H - T_C$ [°C]), the same behaviour can be observed without any load, that is, the output voltage, V_{out}, and current, I_{out}, increases proportionally with the increment of the temperature gradient, ΔT, thus the power output, P_{out}. The linearity between the temperature gradients, $\Delta T = T_H - T_C$ [°C], is also observed which is explained by the linearity observed in the internal resistance, R_{int}, as a function of the test temperature gradient for the thermoelectric module. The red lines ($V_{out,fitted}$) in Figure 10 seem to be parallel to each other, confirming the previous statement. The analysis showed correlation coefficients always above 99.74%, except for the case with the smaller temperature gradient (e.g., for $\Delta T = 5$°C), whose value was 97.55% but still high enough to make the regression lines agree well with the measurements.

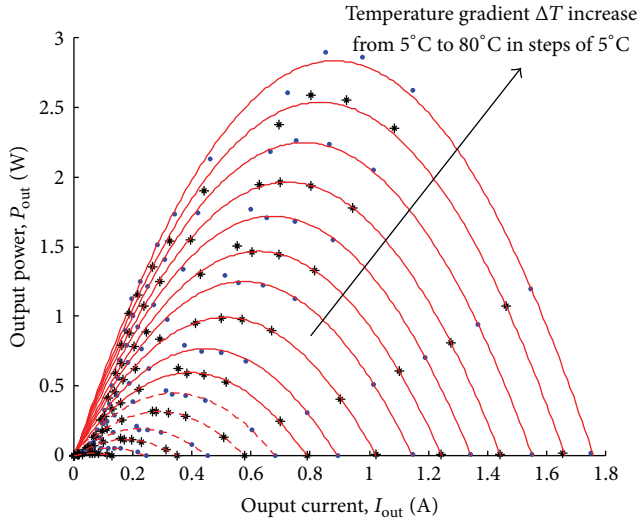

FIGURE 11: The output power, P_{out} [V], versus the output current, I_{out} [A], for different temperature gradient, ΔT [°C].

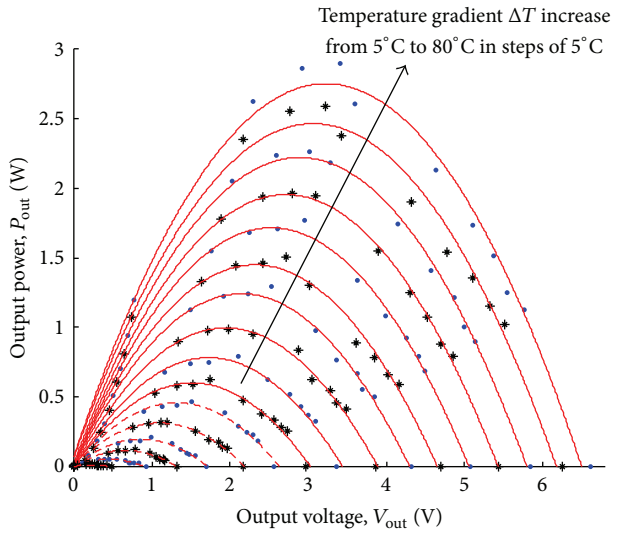

FIGURE 12: The output power, P_{out} [V], versus the output voltage, V_{out} [V], for different temperature gradient, ΔT [°C].

Data analysis revealed that the increase of the temperature gradient, ΔT, lead to a proportional increment of the power output, P_{out} [W], for a fixed load value, R_L [Ω], resulting in $P_{out} = R_L \cdot {I_{out}}^2$ [W]. By conducting the same tests for different fixed load values R_L it is possible to plot the resulting maximum power output curves for the output current I_{out} (Figure 11) and voltage V_{out} (Figure 12) for different temperature gradient values, ΔT. Both in Figure 11 and in Figure 12, the red lines were obtained from the minimum square approximation that resulted in the red lines of Figure 9. In this context, the red plots $P_{out,fitted,1}(I_{out})$ and $P_{out,fitted,2}(V_{out})$ in Figures 11 and 12 were obtained in this manner:

$$P_{out,fitted,1} = I_{out} \times V_{out,fitted}. \quad (2)$$

Additionally, the measured powers P_{out} (blue dots and black stars) were obtained as follows:

$$P_{out}(I_{out}) = I_{out} \times V_{out}. \quad (3)$$

After analysis of the output power curve P_{out} shown in Figures 11 and 12 it is possible to determine the maximum power output as a function of the output voltage V_{out} (V) and output current I_{out} (A) by series module association for different temperature gradient values (ΔT).

4. Conclusions

The assembled monitoring and acquisition system presented a low maximum reading error of ±1.5% for all sampled variables. This was achieved after calibration using precision instruments as reference and by using an accurate temperature monitor and PID controller with a maximum error of ±2°C. Moreover, the file export capability enables the use of more complex data treatment algorithms.

The characterization for the module association was validated by revealing data coherence with data presented in [35]. The series configuration for the two inbC1-127.08HTS modules from Thermoelectric Power Generation is capable of supplying $P_{out} = 2.89$ W for a current of $I_{out} = 850$ mA and voltage $V_{out} = 3.40$ V. The observed load resistance of $V_{out}/I_{out} = 3.99\ \Omega$ is also validated for being contemplated in the interval defined by $[\mu-\sigma, \mu+\sigma]\ \Omega$, where $\mu = R_0 = 3.76\ \Omega$ and $\sigma = \Delta R_{int} = 0.28\ \Omega$.

The use of the assembled monitoring and acquisition system presents itself as a viable option for TEG monitoring and characterization for presenting a low reading error, easy assembly, and low cost. For all of these considerations, this setup is also qualified for academic learning purposes where TEG characterization is desirable.

Conflict of Interests

The authors declare that there is no conflict of interests regarding the publication of this paper.

Acknowledgments

This work was fully supported by the Algoritmi Strategic Project UI 319-2011-2012, under the Portuguese Foundation for Science and Technology Grant Pest C/EEI/UI0319/2011.

References

[1] B. Aksanli, T. S. Rosing, and I. Monga, "Benefits of green energy and proportionality in high speed wide area networks connecting data centers," in *Proceedings of the 15th Design, Automation & Test in Europe Conference & Exhibition (DATE '12)*, pp. 175–180, March 2012.

[2] M. Sithan and L. Loi-Lei, "Application of green technologies in developing countries—reduced carbon emission and conservation of energy," in *Proceedings of the IEEE Power and Energy Society General Meeting*, pp. 1–7, July 2011.

[3] N. Smith and R. McCann, "Investigation of a multiple input converter for grid connected thermoelectric-photovoltaic hybrid system," in *Proceedings of the IEEE Green Technologies Conference*, pp. 1–5, Tulsa, Okla, USA, April 2012.

[4] R. Singh, N. Gupta, and K. F. Poole, "Global green energy conversion revolution in 21st century through solid state devices," in *Proceedings of the 26th International Conference on Microelectronics (MIEL '08)*, pp. 45–54, Niš, Serbia, May 2008.

[5] S. Maharaj and P. Govender, "Waste energy harvesting with a thermoelectric generator," in *Proceedings of the 21st Domestic Use of Energy Conference (DUE '13)*, pp. 1–6, April 2013.

[6] S. Benecke, J. Ruckschloss, N. F. Nissen, and K.-D. Lang, "Energy harvesting on its way to a reliable and green micro energy source," in *Proceedings of the Electronics Goes Green 2012+ (EGG '12)*, pp. 1–8, Berlin, Germany, September 2012.

[7] S. P. Beeby, R. N. Torah, M. J. Tudor et al., "A micro electromagnetic generator for vibration energy harvesting," *Journal of Micromechanics and Microengineering*, vol. 17, no. 7, pp. 1257–1265, 2007.

[8] Z. Wang, V. Leonov, P. Fiorini, and C. van Hoof, "Realization of a wearable miniaturized thermoelectric generator for human body applications," *Sensors and Actuators. Part A: Physical*, vol. 156, no. 1, pp. 95–102, 2009.

[9] A. Khaligh, P. Zeng, and C. Zheng, "Kinetic energy harvesting using piezoelectric and electromagnetic technologiesstate of the art," *IEEE Transactions on Industrial Electronics*, vol. 57, no. 3, pp. 850–860, 2010.

[10] J. Zhao and Z. Yuo, "A shoe-embedded piezoelectric energy harvester for wearable sensors," *Sensors*, vol. 14, no. 7, pp. 12497–12510, 2010.

[11] R. H. Bhuiyan, R. A. Dougal, and M. Ali, "A miniature energy harvesting device for wireless sensors in electric power system," *IEEE Sensors Journal*, vol. 10, no. 7, pp. 1249–1258, 2010.

[12] L. Chen, X. Xu, P. Zeng, and J. Ma, "Integration of energy harvester for self-powered wireless sensor network nodes," *International Journal of Distributed Sensor Networks*, vol. 2014, Article ID 782710, 7 pages, 2014.

[13] M. M. Abbas, M. A. Tawhid, K. Saleem et al., "Solar energy harvesting and management in wireless sensor networks," *International Journal of Distributed Sensor Networks*, vol. 2014, Article ID 436107, 8 pages, 2014.

[14] A. Delnavaz and J. Voix, "Energy harvesting for in-ear devices using ear canal dynamic motion," *IEEE Transactions on Industrial Electronics*, vol. 61, no. 1, pp. 583–590, 2014.

[15] D. Gunduz, K. Stamatiou, N. Michelusi, and M. Zorzi, "Designing intelligent energy harvesting communication systems," *IEEE Communications Magazine*, vol. 52, no. 1, pp. 210–216, 2014.

[16] J.-M. Dilhac and M. Bafleur, "Energy harvesting in aeronautics for battery-free wireless sensor networks," *IEEE Aerospace and Electronic Systems Magazine*, vol. 29, pp. 18–22, 2014.

[17] S. Chamanian, S. Baghaee, H. Ulusan, H. Zorlu, Ö. Külah, and E. Uysal-Biyikoglu, "Powering-up wireless sensor nodes utilizing rechargeable batteries and an electromagnetic vibration energy harvesting system," *Energies*, vol. 7, pp. 6323–6339, 2014.

[18] K. Nguyen, V. H. Nguyen, D. D. Le, Y. Ji, D. A. Duong, and S. Yamada, "ERI-MAC: an energy-harvested receiver-initiated MAC protocol for wireless sensor networks," *International Journal of Distributed Sensor Networks*, vol. 2014, Article ID 514169, 8 pages, 2014.

[19] J. Colomer-Farrarons, P. Miribel-Català, A. Saiz-Vela, M. Puig-Vidal, and J. Samitier, "Power-conditioning circuitry for a self-powered system based on micro PZT generators in a 0.13-μm low-voltage low-power technology," *IEEE Transactions on Industrial Electronics*, vol. 55, no. 9, pp. 3249–3257, 2008.

[20] L. Collins, "Harvest for the world," *IET Power Engineer*, vol. 20, no. 1, pp. 34–37, 2006.

[21] J. Bouchaud and R. Dixon, *Micro-Energy Harvesters: Overview, Applications and Markets*, International Newsletter on Micro Nano Integration, 2008.

[22] D. Dondi, A. Bertacchini, D. Brunelli, L. Larcher, and L. Benini, "Modeling and optimization of a solar energy harvester system for self-powered wireless sensor networks," *IEEE Transactions on Industrial Electronics*, vol. 55, no. 7, pp. 2759–2766, 2008.

[23] L. Mateu and F. Moll, "Appropriate charge control of the storage capacitor in a piezoelectric energy harvesting device for discontinuous load operation," *Sensors and Actuators A: Physical*, vol. 132, no. 1, pp. 302–310, 2006.

[24] G. Min and D. M. Rowe, "Ring-structured thermoelectric module," *Semiconductor Science and Technology*, vol. 22, no. 8, pp. 880–883, 2007.

[25] J. G. Rocha, L. M. Gonçalves, P. F. Rocha, M. P. Silva, and S. Lanceros-Méndez, "Energy harvesting from piezoelectric materials fully integrated in footwear," *IEEE Transactions on Industrial Electronics*, vol. 57, no. 3, pp. 813–819, 2010.

[26] S. Karabetoglu, A. Sisman, Z. Fatih Ozturk, and T. Sahin, "Characterization of a thermoelectric generator at low temperatures," *Energy Conversion and Management*, vol. 62, pp. 47–50, 2012.

[27] W.-H. Chen, C.-Y. Liao, C.-I. Hung, and W.-L. Huang, "Experimental study on thermoelectric modules for power generation at various operating conditions," *Energy*, vol. 45, no. 1, pp. 874–881, 2012.

[28] G. Min and D. M. Rowe, "Conversion efficiency of thermoelectric combustion systems," *IEEE Transactions on Energy Conversion*, vol. 22, no. 2, pp. 528–534, 2007.

[29] J. Martins, L. M. Gonçalves, J. Antunes, and F. Brito, "Thermoelectric exhaust energy recovery with temperature control through heat pipes," *SAE International*, pp. 1–23, 2011.

[30] S. Ashby, J. A. Thomas, J. A. García-Cañadas et al., "Bridging silicon nanoparticles and thermoelectrics: phenylacetylene functionalization," *Faraday Discussions*, 2014.

[31] H. Böttner, J. Nurnus, A. Gavrikov et al., "New thermoelectric components using microsystems technologies," *Journal of Microelectromechanical Systems*, vol. 13, no. 3, pp. 414–420, 2004.

[32] P. M. Attia, M. R. Lewis, C. C. Bomberger, A. K. Prasad, and J. M. O. Zide, "Experimental studies of thermoelectric power generation in dynamic temperature environments," *Energy*, vol. 60, pp. 453–456, 2013.

[33] M. Gomez, R. Reid, B. Ohara, and H. Lee, "Influence of electrical current variance and thermal resistances on optimum working conditions and geometry for thermoelectric energy harvesting," *Journal of Applied Physics*, vol. 113, no. 17, Article ID 174908, 8 pages, 2013.

[34] X. F. Zheng, Y. Y. Yan, and K. Simpson, "A potential candidate for the sustainable and reliable domestic energy generation—thermoelectric cogeneration system," *Applied Thermal Engineering*, vol. 53, no. 2, pp. 305–311, 2013.

[35] S. Maharaj and P. Govender, "A prototype thermoelectric cogeneration unit," in *Proceedings of the 22nd Domestic Use of Energy (DUE '14)*, pp. 1–6, Cape Town, South Africa, April 2014.